[Downloaded from www.aece.ro on Thursday, March 28, 2024 at 13:29:49 (UTC) by 107.21.176.63. Redistribution subject to AECE license or copyright.]

Experimental Method of Determining the Equivalent Circuit Parameters of a Switched Reluctance Machine

Dinko VUKADINOVIĆ, Šime GRBIN, Mateo BAŠIĆ
Faculty of Electrical Engineering, Mechanical Engineering and Naval Architecture in Split, Croatia
dvukad@fesb.hr

***Abstract*—This paper presents an equivalent-circuit-based method to experimentally determine the phase inductance and the iron-loss resistance of a switched reluctance machine (SRM). The proposed equivalent circuit of the SRM phase consists of the winding resistance, the winding inductance and the iron-loss resistance. In this paper, the iron-loss resistance is represented as variable with respect to the phase current, the dc supply voltage and the rotor position. The phase inductance is represented as variable with respect to the phase current and the rotor position. The phase winding resistance is represented by a constant parameter. The proposed method allows estimation of the rotary SRM's iron losses for single-pulse operating regimes.**

***Index Terms*—equivalent circuits, iron losses, inductance measurement, model, switched reluctance machine.**

I. Introduction

A switched reluctance machine (SRM) is an electric machine in which torque is produced by the tendency of its movable part to move to the position where the inductance of the excited winding is maximal, i.e. magnetic reluctance is minimal [1]. The movable part is made of soft magnetic iron and shaped to give the maximum inductance change vs. position. Inherent geometric simplicity, absence of winding or permanent magnets on movable part, lower manufacture cost, reliability and better robustness compared to other electric machines make the SRM a good candidate for various general-purpose adjustable-speed applications [2].

In SRM control systems, two types of control are typically employed - pulse-width-modulation control for low speed applications (PWM mode), and single-pulse control for high speed applications (single-pulse mode). The method proposed in this paper is suitable for the SRMs operating in the single-pulse mode. In this mode, SRMs can operate as generators or as motors, depending on the firing angles.

It is useful to build a model of the SRM to approach various tasks: SRM structure analysis [1, 3-7], SRM losses analysis [8-15], optimization [16] or control [2, 17, 18] of the SRM systems, etc. Conventional SRM models rely on the equivalent resistor-inductor circuit of the SRM and do not include the leakage fluxes, the mutual coupling between the phases or the iron losses [2, 4, 6, 7, 17, 18]. The leakage fluxes and the mutual coupling are usually negligible, whereas the models that include the mutual coupling are complex and require larger computational power [3]. By contrast, the iron losses in single-pulse operating regimes can be up to 50 % of the total losses [15], so they should be taken into account in the SRM model.

Inductance dependence on the phase current and rotor position is usually calculated by the finite element method [5-7] or the flux tube method [4], or estimated from measured electrical quantities [8, 17, 19]. In [8, 17], this dependence is determined experimentally by capturing the transient response of the SRM phase current and voltage during the period of demagnetization. Various other methods are given in [19]. Methods for determination of the iron losses are based either on measurement [8-11] or calculation [11-14]. In the thesis [12], an overview of the current state-of-the-art iron-loss modeling of the SRM is presented in detail.

This paper deals with an equivalent-circuit-based method to experimentally determine the phase inductance and the iron-loss resistance of the SRM [8, 10]. A similar approach is suggested in [20], but neither simulation nor experimental results are provided. The phase inductance and the iron-loss resistance are estimated as in [8]. In [10], the iron losses are determined for the rising and falling flux regions, and for the chopping region. However, in the single-pulse mode, only the rising and falling flux regions are of interest. Furthermore, the method introduced in [10] is applied there for a tubular SRM, whereas in this paper it is for the first time applied for a rotary SRM. In [8], the iron-loss resistance is represented as variable with respect to the iron-loss current, the switching frequency and the rotor position, whereas in [10], it is represented as a function of the phase current, for three different switching frequencies - all for 50 V supply voltage. However, neither of these approaches provides definite description of the iron-loss resistance, so in this paper an attempt is made in this direction by representing the iron-loss resistance as variable with respect to the dc supply voltage, the rotor position and the newly-introduced quasi-rms value of phase current, as defined in Section III B.

II. Proposed Equivalent Circuit of SRM

The equivalent circuit in Fig. 1 represents one phase of a locked-rotor SRM supplied from the asymmetric power converter - the type of converter predominantly used in SRM applications. It comprises two IGBT transistors and two diodes per phase. To account the iron losses, a branch with the iron-loss resistance R_m is connected in parallel with the phase inductance L. The phase winding resistance in Fig. 1 is denoted by R.

Digital Object Identifier 10.4316/AECE.2015.03013

1582-7445 © 2015 AECE

[Downloaded from www.aece.ro on Thursday, March 28, 2024 at 13:29:49 (UTC) by 107.21.176.63. Redistribution subject to AECE license or copyright.]

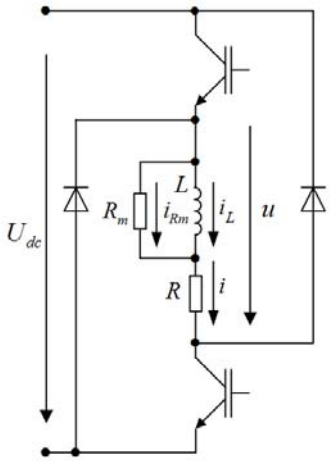

Figure 1. Per-phase SRM equivalent circuit with switching elements of the asymmetric power converter

Fig. 2 shows theoretical waveforms of i_{Rm}, i_L, the phase current i and the induced electromotive force (EMF) e. For convenience, it is assumed that the inductance L, the iron loss resistance R_m and the phase winding resistance R are constant.

At time $t = 0$, the transistors in Fig. 1 are turned on and the SRM phase starts to magnetize. The time interval T_1, during which the SRM phase magnetizes, is described by the following equations:

$$i(t) = i_{Rm}(t) + i_L(t) \tag{1}$$

$$U_{dc} - 2U_T = L\frac{di_L(t)}{dt} + Ri(t) = i_{Rm}(t)R_m + Ri(t) \tag{2}$$

where U_{dc} is the dc supply voltage and U_T is the transistor voltage drop. Since at time $t = 0$ the current i_L cannot start to flow momentarily through the inductance L, the current i flows through the resistances R_m and R, directed by the phase voltage $u = U_{dc} - 2U_T$.

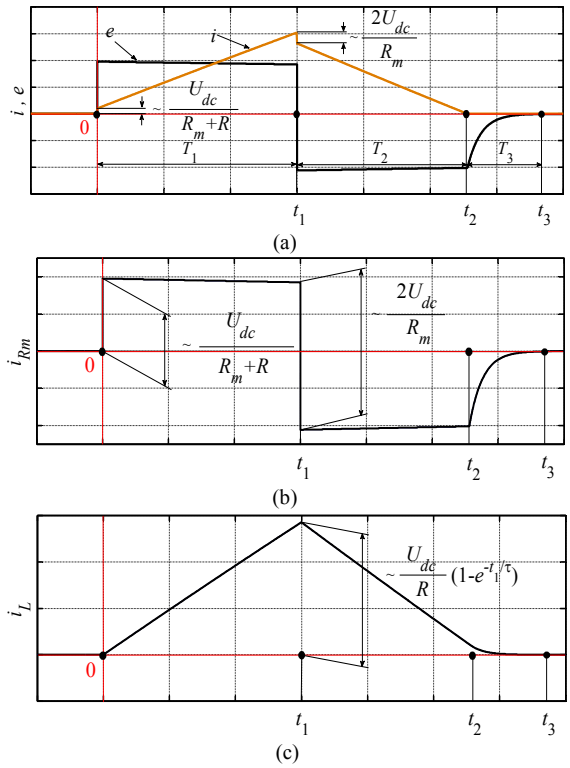

Figure 2. Theoretical waveforms for induced EMF e, phase current i (a), iron-loss current i_{Rm} (b) and inductance current i_L (c)

Therefore, the initial conditions for (1) and (2) are given by the following equations:

$$i_L(0) = 0 \tag{3}$$

$$i(0) = i_{Rm}(0) = \frac{U_{dc} - 2U_T}{R_m + R} \approx \frac{U_{dc}}{R_m + R} \tag{4}$$

From (1) - (4) it follows:

$$i(t) = -\frac{(U_{dc} - 2U_T)R_m}{R(R_m + R)}\mathrm{e}^{-\frac{t}{\tau}} + \frac{U_{dc} - 2U_T}{R} \tag{5}$$

$$i_{Rm}(t) = \frac{U_{dc} - 2U_T}{R_m + R}\mathrm{e}^{-\frac{t}{\tau}} \tag{6}$$

$$i_L(t) = \frac{U_{dc} - 2U_T}{R}\left(1 - \mathrm{e}^{-\frac{t}{\tau}}\right) \tag{7}$$

$$e(t) = \frac{(U_{dc} - 2U_T)R_m}{R_m + R}\mathrm{e}^{-\frac{t}{\tau}} \tag{8}$$

where τ is the time constant $\tau = L(R+R_m)(R_mR)^{-1}$.

The time interval T_2 begins at time t_1 by turning off the transistors, which in turn initiates demagnetization of the SRM phase. The energy stored in the phase coil is returned to the dc power-supply trough diodes. Both the phase current and the inductance current continue to flow in the same direction (Figs. 2a and 2c) and gradually fall to zero. The EMF, however, changes polarity because of the fall of the magnetic flux in the phase coil, so the iron-loss current changes direction (Fig. 2b)

The inductance current cannot change momentarily so it must be $i_L(t_1^-) = i_L(t_1^+)$, i.e., $\Delta i_L = i_L(t_1^+) - i_L(t_1^-) = 0$. Hence, according to (1), the phase current change is

$$\Delta i = \Delta i_{Rm} + \Delta i_L = \Delta i_{Rm} \tag{9}$$

$$\Delta i = i(t_1^+) - i(t_1^-) = i_{Rm}(t_1^+) - i_{Rm}(t_1^-) \tag{10}$$

At time t_1^-, while transistors still conduct, the iron-loss current is

$$i_{Rm}(t_1^-) = \frac{U_{dc} - 2U_T - Ri(t_1^-)}{R_m} \tag{11}$$

and at time t_1^+, the supply voltage U_{dc} changes sign from the perspective of the phase winding so the iron-loss current is

$$i_{Rm}(t_1^+) = \frac{-U_{dc} - 2U_D - Ri(t_1^+)}{R_m} \tag{12}$$

where U_D is the diode voltage drop.

From (9)-(12), at time t_1, both the phase current and the iron-loss current change for

$$\Delta i = \frac{-2U_{dc} - 2(U_D - U_T)}{R_m + R} \tag{13}$$

Since U_D and U_T are almost equal and R_m is much larger than R, the current change can be approximated as

$$\Delta i \approx \frac{-2U_{dc}}{R_m} \tag{14}$$

Equations that describe the demagnetization time interval T_2 are (1) and

$$-U_{dc} - 2U_D = L\frac{di_L(t)}{dt} + Ri(t) = i_{Rm}(t)R_m + Ri(t) \tag{15}$$

whereas the initial conditions for this time interval are

[Downloaded from www.aece.ro on Thursday, March 28, 2024 at 13:29:49 (UTC) by 107.21.176.63. Redistribution subject to AECE license or copyright.]

$$i(t_1^-) = -\frac{(U_{dc} - 2U_T)R_m}{R(R_m + R)} e^{-\frac{t_1}{\tau}} + \frac{U_{dc} - 2U_T}{R} \quad (16)$$

$$i_{Rm}(t_1^-) = \frac{U_{dc} - 2U_T}{R_m + R} e^{-\frac{t_1}{\tau}} \quad (17)$$

$$i_L(t_1^-) = \frac{U_{dc} - 2U_T}{R}\left(1 - e^{-\frac{t_1}{\tau}}\right) \quad (18)$$

From (1) and (15)-(18), the following equations are obtained for the time interval T_2:

$$i(t) = -\left(i_{Rm}(t_1^-) - \frac{2U_{dc}}{R_m}\right)\frac{R_m}{R} e^{-\frac{t}{\tau}} + K \quad (19)$$

$$i_{Rm}(t) = \left(i_{Rm}(t_1^-) - \frac{2U_{dc}}{R_m}\right) e^{-\frac{t}{\tau}} \quad (20)$$

$$i_L(t) = -\left(i_{Rm}(t_1^-) - \frac{2U_{dc}}{R_m}\right)\frac{R + R_m}{R} e^{-\frac{t}{\tau}} + K \quad (21)$$

$$e(t) = \left(i_{Rm}(t_1^-) - \frac{2U_{dc}}{R_m}\right) R_m e^{-\frac{t}{\tau}} \quad (22)$$

where $K = i(t_1^-) - i_{Rm}(t_1^-) + \left(i_{Rm}(t_1^-) - \frac{2U_{dc}}{R_m}\right)\frac{R + R_m}{R}$

The time interval T_3 begins at time t_2 when the phase current reaches zero

$$t_2 = \tau \ln \frac{i_{Rm}(t_1^-)R_m - 2U_{dc}}{KR} \quad (23)$$

During this interval i_L and i_{Rm} are equal and fall to zero

$$i_{Rm}(t) = -i_L(t) = \left(i_{Rm}(t_1^-) - \frac{2U_{dc}}{R_m} e^{-\frac{t_2}{\tau}}\right) e^{-\frac{t}{\tau_1}} \quad (24)$$

whereas induced EMF equals

$$e(t) = \left(i_{Rm}(t_1^-) - \frac{2U_{dc}}{R_m} e^{-\frac{t_2}{\tau}}\right) R_m e^{-\frac{t}{\tau_1}} \quad (25)$$

where $\tau_1 = LR_m^{-1}$.

The remaining stored magnetic energy is dissipated in the iron core, i.e., the phase inductance and the iron-loss resistance work as *RL*-circuit.

III. Determination of Equivalent Circuit Parameters

The schematic diagram of the measurement setup is given in Fig. 3. In each experiment, the phase current is measured on one channel of the data acquisition system (DAS), whereas either the phase voltage or the induced EMF is measured on the other channel, as depicted by the dashed lines in Fig. 3. The transistors from Fig. 1 are represented by the switch *S*.

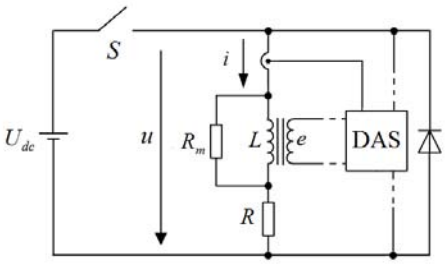

Figure 3. Schematic diagram of the measurement setup

A. Phase inductance estimation

The phase inductance L is obtained experimentally by using the dc excitation method, i.e., by locking the rotor in a desired position while making the measurements for different values of the dc phase current. The procedure is repeated at various rotor positions. Note that it is necessary to know the inductance dependence on the rotor position and phase current to calculate the SRM's rotational EMF.

When the switch S is closed, the phase current i is increased slowly, e.g., by means of the variable resistor, until the required constant dc current I_{dc} flows in the phase winding. When the switch S is opened, the energy stored in the winding is dissipated as heat in the phase winding resistance R and the iron-loss resistance R_m. Induced EMF e is calculated form the measured phase current i and phase voltage u as follows:

$$e(t) = \frac{d\Psi(t)}{dt} = -(u(t) - i(t)R) \quad (26)$$

Then, the flux linkage is calculated by integrating the induced EMF. The phase winding resistance R should be measured just before each experiment to compensate for the resistance thermal change. Alternatively, the EMF can be directly measured by placing a search coil in the SRM phase (Fig. 4). It should be noted that this method assumes that the search coil links all flux produced by the main phase coil.

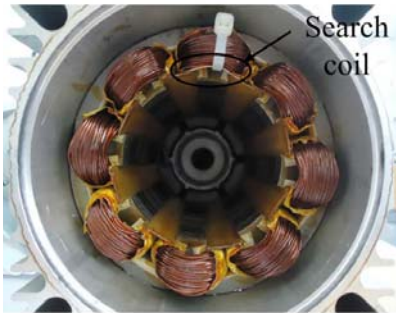

Figure 4. Photo of the stator windings with the search coil

The phase inductance is calculated as

$$L = \frac{\Psi}{I_{dc}} \quad (27)$$

Since the phase inductance depends on both the rotor position θ and the phase current, the measurements should be repeated for different values of I_{dc} and θ.

B. Iron-loss resistance estimation

According to [15], hysteresis losses, classical eddy current losses and excess losses are responsible for iron losses. The hysteresis losses result from changes in flux density and magnetic field of the iron. The eddy-current losses are produced by circulation of parasitic eddy currents through iron and are dictated by changes in flux density over time. The excess losses are caused by the movement of the magnetic-domain walls and domain rotation damped by the eddy currents. Same as the eddy-current losses, the excess losses are dictated by changes in flux density over time.

Summed up, the iron losses depend on the flux linkage value and rate of change. The flux linkage value is a function of the phase current and the phase inductance, which is in turn a function of the phase current and the rotor position. From (26), the rate of change of the flux linkage is

[Downloaded from www.aece.ro on Thursday, March 28, 2024 at 13:29:49 (UTC) by 107.21.176.63. Redistribution subject to AECE license or copyright.]

a function of the phase current and the phase voltage.

To determine the equivalent iron-loss resistance, several periodic experiments need to be performed in which the transistors in Fig. 1 are switched on during the time interval T_1 (rising flux region) and switched off during the time interval T_2 (falling flux region), while keeping the voltage U_{dc} constant. The iron-loss resistance is then calculated as follows

$$R_m = \frac{E^2}{P_{Fe}} \tag{28}$$

where E is the rms value of the induced EMF, which is obtained either by means of the search coil or from (26) after measuring u, i and R

$$E = \sqrt{\frac{1}{T}\int_0^T e^2(t)dt} \tag{29}$$

In (29), T denotes the switching period and P_{Fe} in (28) represents the iron losses per phase and is given by [10]

$$P_{Fe} = \frac{1}{T}\int_0^T i_{Rm}(t)e(t)dt = \frac{1}{T}\int_0^T i(t)e(t)dt - \frac{1}{T}\int_0^T i_L(t)e(t)dt \tag{30}$$

Since the second term on the right hand side of (30) is zero, the iron losses per phase are

$$P_{Fe} = \frac{1}{T}\int_0^T i(t)e(t)dt \tag{31}$$

Note that the iron losses are calculated by integrating the product of two measurable quantities: i and e.

Form (28)-(31) it follows:

$$R_m = \frac{\frac{1}{T}\int_0^T e^2(t)dt}{\frac{1}{T}\int_0^T i(t)e(t)dt} = \frac{\int_0^{T_q} e^2(t)dt}{\int_0^{T_q} i(t)e(t)dt} \tag{32}$$

where $T_q = T_1 + T_2 + T_3$ is the time interval during which the iron losses can possibly exist since $e \neq 0$.

Everything that happens after t_3 and until the end of the switching period does not contribute to the iron losses, provided that $T_q < T$, which is always fulfilled in practice. Otherwise, if the transistors are switched on again before T_q has passed, machine can be damaged due to the continuous dc current component that would emerge [21]. This mode is known as continuous conduction operating mode.

From (32) it follows that R_m does not depend on the switching period (Fig. 8). Consequently, the rms value of the phase current, being dependent on the switching period, cannot be used to uniquely describe the iron-loss resistance. Instead, use of the quasi-rms value of the phase current, restricted to the time interval T_q, is proposed. The quasi-rms value of the phase current $I_{q\text{-}rms}$ is given by

$$I_{q\text{-}rms} = \sqrt{\frac{1}{T_q}\int_0^{T_q} i^2(t)dt} \tag{33}$$

The quasi-average value of the phase current, restricted to the same time interval, could be defined as well. However, the total losses are usually expressed as a function of the rms value, so the quasi-rms value allows easier transition between the two in the case when the total losses are to be estimated. Namely, if the time intervals T and T_q are known, then

$$I_{q-rms}^2 = \frac{T}{T_q} I^2 \tag{34}$$

Summed up, the iron-loss resistance depends on the rotor position, the quasi-rms value of the phase current and the induced EMF. So, in order to accurately determine the corresponding characteristics, the measurements should be taken for different values of all three variables within the respective ranges of interest.

The rotor position θ is easily accurately measured by means of a digital encoder. The quasi-rms value of the phase current $I_{q\text{-}rms}$ can be determined from the phase current measured by a current sensor. Measurement of the induced EMF e by means of a search coil is impractical because it requires opening of the machine and mounting a search coil (an additional sensor), as described in Section III A. Considering the potential application of the proposed SRM model for control system design, whose practical implementation would inevitably require mounting a certain number of sensors for online measurements, any additional sensors should be avoided. Since i and U_{dc} are anyway measured in SRM control systems, the method based on (26) is in this respect preferred. Moreover, according to Fig. 3, the SRM phase voltage u in (26) can be replaced by U_{dc} since u is normally much higher than the voltage drops across the semiconductors. Taking this one step further, U_{dc} can be used instead of e to represent the iron-loss resistance since the voltage drop across the phase winding resistance is normally negligible compared to e. In this paper, the iron-loss resistance is expressed as $R_m = R_m(I_{q\text{-}rms}, U_{dc}, \theta)$.

IV. Experimental Results

To experimentally determine the parameters of the proposed equivalent circuit, the laboratory setup was designed as in Fig. 3. The main components of the laboratory setup are as follows: the switched reluctance machine (parameters provided in Appendix); dSpace DS1104 R&D controller board, used for switching of the IGBT transistor and acquisition of data necessary for the phase inductance estimation; the oscilloscope type TDS1012B, manufactured by Tektronix, used for acquisition of data necessary for the iron-loss resistance estimation; the incremental rotary encoder, type XCC 1510PS50X, manufactured by Telemecanique, used for identification of the rotor angle; the current transducer, type LA 55-P, manufactured by LEM, used for acquisition of the phase current; the voltage transducer, type LV 25-P, also manufactured by LEM, used for acquisition of the induced EMF in the search coil with 8 turns, mounted over the stator pole. Note that the DSP was used for the IGBT switching because it was available, but a simpler and probably less expensive analog or digital switching device could have been used instead.

A. Phase inductance experimental results

In this paper, the EMF is calculated based on (26), as described in Section III A. It has to be noted, however, that several test measurements were taken with the search coil to

[Downloaded from www.aece.ro on Thursday, March 28, 2024 at 13:29:49 (UTC) by 107.21.176.63. Redistribution subject to AECE license or copyright.]

verify the accuracy of the chosen method, only to discover that the EMF responses obtained from the two methods are practically overlapping. The DSP was used for data acquisition, but the oscilloscope could have been used instead. To avoid ripple, the dc supply voltage U_{dc} was acquired from four 12 V batteries connected in series. The measurements were taken at the rotor position intervals of 1º between 0º and 30º, and at the phase current intervals of 1 A, up to 9 A, as suggested in [17]. The obtained flux-linkage profile and the phase inductance profile are shown in Figs. 5 and 6, respectively.

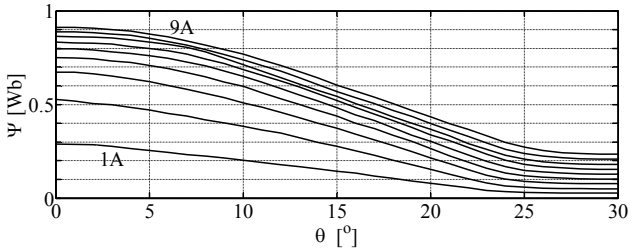

Figure 5. Flux-linkage profile with respect to phase current and rotor position

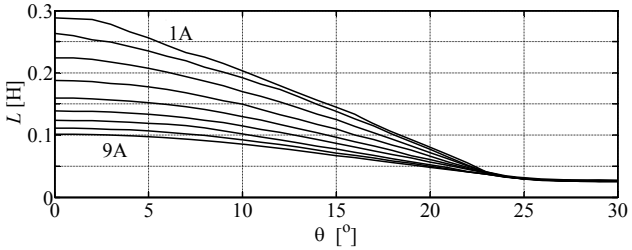

Figure 6. Phase inductance profile with respect to phase current and rotor position

When the rotor pole is aligned with the stator pole (position 0º), both the flux linkage and the inductance have maximum values for a given phase current. As the rotor pole advances to the fully unaligned position (position 30º), the magnetic flux path through the air gets longer, which leads to an increase in the magnetic reluctance. Consequently, both the flux linkage and the phase inductance descend. At positions 25º to 30º, the phase inductance is almost constant (Fig. 6). As the phase current rises, the machine gets saturated, as can be seen in Fig. 5. For the machine used in this paper, the currents above 9 A have no notable effect on the flux linkage or the phase inductance.

B. Iron-loss resistance experimental results

To estimate the iron-loss resistance values, several periodic experiments were performed. In this case, the dc supply voltage U_{dc} was acquired by an autotransformer and a 3-phase diode bridge rectifier, whereas the residual ac component was filtered out by means of the capacitor $C = 5$ mF. Note that in this case it was impractical to use the 12 V batteries because a large number of them would have to be connected in series to obtain the required dc supply voltage. In addition, the oscilloscope was used for data acquisition instead of the DSP to achieve the sufficient measurement accuracy. Namely, because the iron-loss resistance estimation relies on the integration of the EMF squared in the numerator of (32), the EMF should be measured with the highest possible sample rate. Maximum sample rates achieved by the oscilloscope ranged from 100 kHz to 2.5 MHz, which is much higher than the rates achievable by DS1104.

Fig. 7 shows the measured waveforms of the EMF and the phase current in the aligned position, for the phase current peak values of 2 A and 10 A and the dc supply voltage of 200 V. The waveforms shown in Fig. 7a are similar to those in Fig. 2, which is due to the negligible magnetic saturation, i.e., low value of the phase current. By contrast, in Fig. 7b, the inductance change due to the magnetic saturation is evident from the phase current slope.

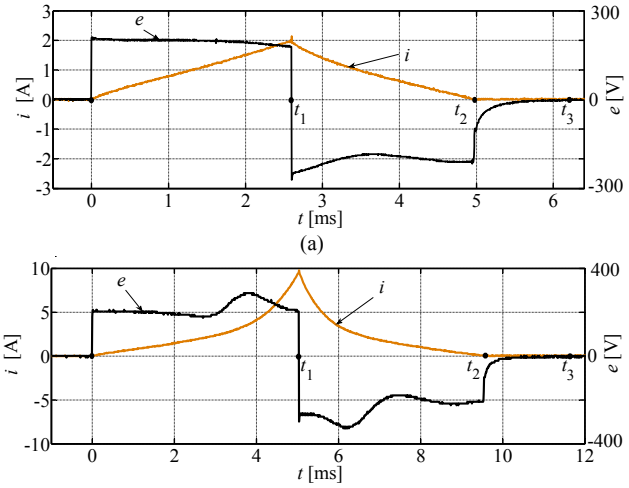

Figure 7. Measured induced EMF and phase current in the aligned position, maximal phase current 2 A (a) and 10 A (b) and U_{dc} = 200 V

Also note in Fig. 7 that during the time interval t_2-t_3 the phase current is zero, while the induced EMF is not, which is in accordance with the theoretical analysis presented in Section II. This is important because it confirms the correctness of placing the iron-loss resistance in parallel with the phase inductance, as in Fig. 1. Similar experimental waveforms were obtained for other values of the supply voltage, the rotor position and the phase currents.

Eq. (32) anticipates that R_m should not be affected by the switching frequency, provided that the switching period is larger than T_q. To check this, the experiment was performed in which the values of $I_{q\text{-}rms}$, U_{dc} and θ were held constant while the switching frequency was varied. The obtained results confirmed the above hypothesis and are shown in Fig. 8 (observed deviations are within the measurement error of the used equipment).

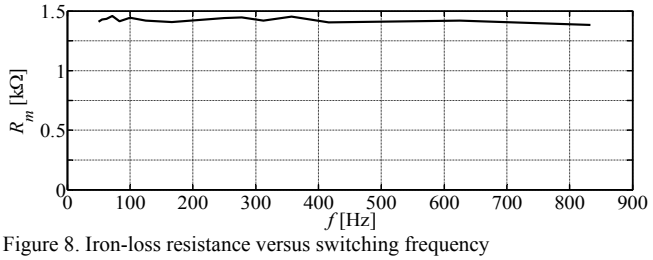

Figure 8. Iron-loss resistance versus switching frequency

Series of experiments were conducted to determine the dependence of R_m on the quasi-rms phase current, the rotor position and the dc supply voltage. The measurements were taken at the rotor position intervals of 5º between 0º and 25º and at three different levels of the dc supply voltage: U_{dc} = 100 V, U_{dc} = 150 V and U_{dc} = 200 V. Different quasi-rms values of the phase current for the same U_{dc} were achieved by changing T_1. Fig. 9 shows the obtained results.

[Downloaded from www.aece.ro on Thursday, March 28, 2024 at 13:29:49 (UTC) by 107.21.176.63. Redistribution subject to AECE license or copyright.]

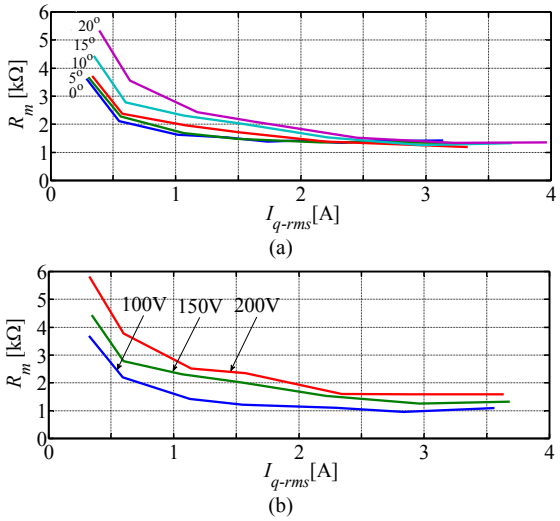

Figure 9. Iron-loss resistance versus $I_{q\text{-}rms}$ for: (a) various rotor positions and 150 V supply voltage, (b) various supply voltages and 15º rotor position

This figure shows that the iron-loss resistance significantly depends on $I_{q\text{-}rms}$ in the low-value region of $I_{q\text{-}rms}$, whereas in the high-value region of $I_{q\text{-}rms}$, the iron-loss resistance is not much affected by $I_{q\text{-}rms}$ and tends to have a constant value, which is due to the magnetic saturation.

In addition, the iron-loss resistance increases with θ for the same $I_{q\text{-}rms}$ value (Fig. 9a). This is explained by the fact that increased θ really means increased misalignment, and thus increased reluctance. In addition, by increasing the dc supply voltage, the induced EMF is also increased. Since the numerator in (32) then grows faster than the denominator, the iron-loss resistance is also increased (Fig. 9b).

V. Conclusion

In this paper, the experimental method for estimation of the phase inductance and the iron-loss resistance of a rotary SRM is successfully applied. The proposed method does not involve complex calculations and does not require information about the machine geometry and materials. In addition, it allows estimation of the phase inductance and the iron-loss resistance on the basis of easily measured variables. The obtained phase inductance profile and iron-loss resistance characteristics are independent of the switching frequency and can be used as input data for the SRM simulations. The drawback of the proposed method is that it requires data acquisition equipment with high sampling rate, but this condition is easily met by means of the standard digital oscilloscope. The future research is aimed at development of the SRM simulation model and its control system based on the proposed equivalent circuit.

Appendix

Parameters of the 8/6 SRM: 1.1 kW, 6 A, 2000 r/min, stator outer diameter 135 mm, stator inner diameter 80 mm, rotor diameter 79.5 mm, stator arc 22º, rotor arc 24º, air gap length 0.25 mm, number of windings per phase 300.

References

[1] T. J. E. Miller, "Optimal Design of Switched Reluctance Motors," IEEE Trans. Industrial Electronics, vol. 49, no. 1, pp. 15-27, Feb. 2002. doi:10.1109/41.982244

[2] P. Asadi, M. Ehsani, B. Fahimi, "Design and control characterization of switched reluctance generator for maximum output power," in *Applied Power Electronics Conference and Exposition*, Dallas, 2006, pp. 1639-1644. doi:10.1109/APEC.2006.1620761

[3] A. Fleury, R. J. Dias, W. R. H. Araujo, A. W. F. V. Silveira, D. A. Andrade, G. C. Ribeiro, "Effects of Mutual inductances on the Switched Reluctance Machines," in *International Conference on Renewable Energies and Power Quality*, Santiago de Compostela (Spain), 2012, pp. 28-30.

[4] A. E. Santo, M. R. Calado, C. Cabrita, "Static Simulation of a Linear Switched Reluctance Actuator with the Flux Tube Method," Advances in Electrical and Computer Engineering, vol. 10, no. 2, pp. 35-42, 2010. doi:10.4316/AECE.2010.02006

[5] E. K. Beser, S. Camur, B. Arifoglu, E. Beser, "Design and Analysis of an Axially Laminated Reluctance Motor for Variable-Speed Applications," Advances in Electrical and Computer Engineering, vol. 13, no. 1, pp. 75-80, 2013. doi:10.4316/AECE.2013.01013

[6] A. Mosallanejad, A. Shoulaie, "Investigation and Calculation of Magnetic Field in Tubular Linear Reluctance Motor Using FEM," Advances in Electrical and Computer Engineering, vol. 10, no. 4, pp. 43-48, 2010. doi:10.4316/AECE.2010.04007

[7] N. C. Lenin, R. Arumugam, V. Chadresekar, "Force Profiles of a Linear Switched Reluctance Motor Having Special Pole Face Shapes," Advances in Electrical and Computer Engineering, vol. 10, no. 4, pp. 129-134, 2010. doi:10.4316/AECE.2010.04021

[8] D. Vukadinović, Š. Grbin, M. Bašić, "Novel Equivalent Circuit of Switched Reluctance Machine with Iron Losses," in *4th European Conference for the Applied Mathematics and Informatics (AMATHI '13)*, Dubrovnik, 2013, pp. 195-199.

[9] J. Corda, S. M. Jamil, "Inclusion of eddy currents impact in the model of a switched reluctance machine based on the equivalent electric circuit," Electrical Engineering Electronic Journal, vol. 1, 2013.

[10] J. Corda, M. J. Shabbir, "Experimental Determination of Equivalent-Circuit Parameters of a Tubular Switched Reluctance Machine With Solid-Steel Magnetic Core," IEEE Trans. Industrial Electronics, vol. 57, no. 1, pp. 304-310, 2010. doi:10.1109/TIE.2009.2026762

[11] J. Faiz, B. Ganji, P. Pillay, C. Yicheng, "Analytical core loss model for the switched reluctance motor with experimental verification," in *The 9th International Conference on Optimization of Electrical and Electronic Equipment*, Brasov (Romania), 2004, pp. 47-52.

[12] J. A. Walker, Aspects of magnetization and iron loss characteristics in switched-reluctance and permanent-magnet machines, PhD thesis, University of Glasgow, pp. 124-141, 2006.

[13] V. Raulin, A. Radun, I. Husain, "Modeling of losses in switched reluctance machines," IEEE Trans. Industry Applications, vol. 40, no. 6, pp. 1560-1569, 2004. doi:10.1109/TIA.2004.836225

[14] J. T. Charton, J. Corda, J. M. Stephenson, S. P. Randall, "Dynamic modelling of switched reluctance machines with iron losses and phase interactions," IEE Proceedings – Electric Power Applications, vol. 153, no. 3, pp. 327-336, May. 2006. doi:10.1049/ip-epa:20050454

[15] M. Torrent, P. Andrada, B. Blanqué, E. Martinez, Perat J. I. Perat, J. A. Sanchez, "Method for estimating core losses in switched reluctance motors," European Trans. Electric Power, vol. 21, no 1, pp. 757-771, 2010. doi:10.1002/etep.475

[16] G. Venkatesan, R. Arumugam, "Power Factor Improvement in Switched Reluctance Motor Drive," Advances in Electrical and Computer Engineering, vol. 10, no. 1, pp. 59-62, 2010. doi:10.4316/AECE.2010.01010

[17] S. K. Sahoo, High-performance torque control of switched reluctance motor, PhD thesis, Department of electrical and computer engineering, National University of Singapore, pp. 33-36, 2006.

[18] A. Tahour, H. Abid, A. G. Aissaoui, "Speed Control of Switched Reluctance Motor Using Fuzzy Sliding Mode," Advances in Electrical and Computer Engineering, vol. 8, no. 1, pp. 21-25, 2008. doi:10.4316/AECE.2008.01004

[19] K.Y. Lu, P.O. Rasmussen, A.E. Ritchie, "Investigation of Flux Linkage Profile Measurement Methods for Switched Reluctance Motors and Permanent Magnet Motors," IEEE Trans. Instrumentation and Measurements, vol. 58, no. 9, pp. 3191-3198, 2009. doi:10.1109/TIM.2009.2017154

[20] V. V. Athani, V. N. Walivadekar, "Equivalent circuit for switched reluctance motor," Electric Machines & Power Systems, vol. 22, no. 4, pp. 533-543, 1994. doi:10.1080/07313569408955585

[21] P. Asadi, Development and Application of an Advanced Switched reluctance Generator Drive, PhD thesis, Texas A&M University, pp. 34-37, 2006.